

20 p.
Code 1 N64-25688
CR 56516 Cat 15

Technical Report No. 32-573

*A Normal-Incidence Reflective Polariscopes
for Viscoelasticity Measurements*

*Anthony San Miguel
Robert H. Silver*

OTS PRICE

XEROX

\$

MICROFILM

\$

jpl

JET PROPULSION LABORATORY
CALIFORNIA INSTITUTE OF TECHNOLOGY
PASADENA, CALIFORNIA

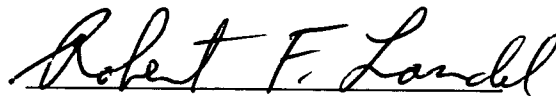
June 1, 1964

Technical Report No. 32-573

***A Normal-Incidence Reflective Polariscopes
for Viscoelasticity Measurements***

Anthony San Miguel

Robert H. Silver

A handwritten signature in cursive script, reading "Robert F. Landel". The signature is written in dark ink and is positioned above a horizontal line.

Robert F. Landel, Chief
Polymer Research Section

**JET PROPULSION LABORATORY
CALIFORNIA INSTITUTE OF TECHNOLOGY
PASADENA, CALIFORNIA**

June 1, 1964

Copyright © 1964
Jet Propulsion Laboratory
California Institute of Technology

Prepared Under Contract No. NAS 7-100
National Aeronautics & Space Administration

CONTENTS

I. Introduction	1
II. Theoretical Aspects	2
A. A Shear-Difference Method	3
B. A Method Peculiar to Incompressible Coatings	4
C. Comparison of the Methods	5
III. Description of the Apparatus	6
A. Xenon Flashtube Light Source	7
B. Filter-Indexing Mechanism	8
C. Camera Selection	10
D. Program Timing	11
E. Apparatus Summary	11
IV. An Illustrative Example and Discussion	11
V. Conclusion	13
Nomenclature	13
References	14

TABLE

1. Biaxial strains obtained by three methods	5
---	---

FIGURES

1. The deformation of an unrestricted, thick-walled cylinder of solid propellant, by internal pressurization	3
2. Two semicoatings of differing sensitivity	4
3. Exploded view of polariscope	6
4. Torus xenon flashtube and reflector	6
5. Reflective polariscope arrangement	7
6. Variously oriented Polaroid filters mounted on an indexing disk	8

FIGURES (Cont'd)

7. Polariscope with associated instrumentation	9
8. Electrical schematic of polariscope	10
9. Spectral energy distribution curve of a typical xenon-filled flashtube	10
10. Spectral energy distribution of xenon-filled tubes under normal loading	10
11. Time—light curves for a flashtube at various capacitance and voltage levels	10
12. Circumferential, radial, and longitudinal strains vs. time	12

ABSTRACT

25688

A normal-incidence reflective polariscope, together with some auxiliary instrumentation, is described. The instrument consists of eight unit polariscopes, suitably oriented, which are indexed into position within a short period of time to obtain a set of eight data. The data obtained provide sufficient information to separate the principal strains obtained at different time intervals. The primary experimental objective was to design an inflated cylinder test, analogous to the loading experienced in a solid propellant rocket, that would enable reasonable measurements of the triaxial surface-layer strains of a viscoelastic material as a function of time. The stress geometry imposed on the viscoelastic material was that of an unrestricted, internally pressurized, thick-walled tubular cylinder. The material investigated was polyurethane solid propellant. Two different methods to reduce the biaxial strains in a low-modulus birefringent polyurethane coating are also described.

Author

I. INTRODUCTION

A solid propellant such as a composite ammonium perchlorate polyurethane will readily deform (creep) as a function of time under moderate, constant loading. The experimental knowledge of this functional relationship is prerequisite to future theoretical considerations (Ref. 1, 2, 3) regarding mechanical property studies as well as to applied design problems (Ref. 4). The peculiarity of solid propellant has required that current displacement- and strain-measuring techniques be modified or improved.

Polyurethane propellant appears physically similar to a hard, opaque rubber that is capable of both elastic and viscoelastic response at ambient temperature, depending upon the environment. This composite propellant is highly filled with minute oxidizer crystals and fine metal

powder. The initial elastic-tension modulus may be of the order of 500 to 1,000 psi. The load-strain curve is usually nonlinear in the elastic regime. The mode of this curve is similar to that of a total load-strain curve for a ductile metal. The maximum stress may be of the order of 100 psi, whereas the maximum useful strain may be of the order of 30 percent. The material is essentially homogeneous and isotropic for small loadings. This may not be true for moderate to high loadings, since a dewetting mechanism (separation of filler from binder) becomes predominant.

One method to measure the principal biaxial viscoelastic strains on the flat surface of a thick-walled cylinder end, for example, is to use a photoelastic-coating

technique (Ref. 5, 6, 7). By using a low-modulus (less than 500 psi) birefringent resin (Ref. 8), the reinforcement may be minimized. Other related measurement discrepancies can likewise be accounted for to correct the final strain readings (Ref. 6, 9, 10, 11, 12). An approximate third principal viscoelastic "strain" may be measured by observing the over-all change of the longitudinal dimension. Here it is assumed that a pressurized, unrestricted, thick-walled cylinder contracts uniformly. This assumption is questionable. However, since the circumferential and radial strains are larger than the longitudinal strain, the discrepancy introduced is not considered intolerable. A problem arises when the photoelastic-coating technique is used to measure time-

dependent strains, in that the position of both the isoclinics and isochromatics must be recorded as a function of time. One solution to this problem, presented here, simply requires that a number of preset polariscopes be indexed so as to record the isoclinics in a short period (ideally an instant) of time. In this manner, groups of readings may be taken at different intervals of time. The extension of this experimentation to the temperature or dynamic loading regime (inertia being significant) is not discussed in this Report. However, the experimental philosophy presented (isoclinics and isochromatics as a function of time) is directly applicable to such studies as those of photoviscoelastic (Ref. 13) and photothermoelastic relationships (Ref. 14).

II. THEORETICAL ASPECTS

One objective in a mechanical properties study is to measure the individual principal stresses and strains in an infinitesimal region subjected to an environmental restraint. In this manner, constitutive equations may be postulated on the basis of the experimentally observed relationships between stresses and strains.

The photoelastic coating technique may be used to measure surface strains and their associated principal directions. The technique consists of recording the stress-strain-optic relationship within a birefringent coating bonded to the surface of the material under inspection. If the coating behaves as an elastic plane-stress structure, the strain state can be computed using the classical photoelastic theory. The surface strain state of the material under inspection must be reasonably the same as that of the bonded coating. Various reinforcement corrections may then be employed to improve the accuracy of the strain measurements.

Two methods to reduce the principal strains in an incompressible elastic coating are discussed below. These methods are applicable because the polyurethane coating used behaves as an ideal rubber, i.e., it is incom-

pressible. However, it is noted that there are other methods available. The methods described below are particularly suitable for the experiment considered in this Report and are based on the following assumptions, which have been experimentally verified (Ref. 6, 15).

1. The stress-strain-optic relationship for an elastic polyurethane coating can reasonably be stated as

$$\begin{aligned} n_{11} - n_{22} &= 2tK (\epsilon_{11} - \epsilon_{22}) \\ &= 2tC (\sigma_{11} - \sigma_{22}) \end{aligned} \quad (1)$$

where

$$\begin{aligned} K &= \frac{CE}{1 + \mu} \\ t &= t_0 (1 + e_{33}) \end{aligned}$$

2. The coating is linearly elastic to 30% strain; hence the linear constitutive equations are

$$\sigma_{ij} = m_{ijkl} \epsilon_{kl} \quad (2)$$

3. The body forces within the coating are negligible; thus the equilibrium equations are

$$\sigma_{ij,i} = 0 \quad (3)$$

4. Shear gradients do not traverse the thickness of the coating except near the free edges. Hence

$$\frac{\partial \sigma_{zx}}{\partial z} \approx \frac{\partial \sigma_{zy}}{\partial z} \approx 0 \quad (4)$$

A. A Shear-Difference Method

With the assumptions given above, the equilibrium equations (Eq. 3) become

$$\frac{\partial \sigma_{xx}}{\partial x} + \frac{\partial \sigma_{yx}}{\partial y} = 0 \quad (5)$$

$$\frac{\partial \sigma_{xy}}{\partial x} + \frac{\partial \sigma_{yy}}{\partial y} = 0$$

These equations indicate that the coating responds in a manner similar to that of a classical plane photoelastic model. Therefore, the theory and techniques applicable to classical photoelastic models can be used to explain the behavior of photoelastic coatings.

The structure chosen for analysis was that of an unrestricted thick-walled cylinder subjected to an internal pressure as shown in Fig. 1. The point region under investigation is at the center of the coating. Two semi-circular coatings of differing sensitivities are bonded to the flat end-surface of the propellant cylinder (Fig. 2). Note that there is no shear along any radial trace for a pressurized cylinder, because of symmetry. Therefore, the classical shear equation reduces to

$$\sigma_{\psi} = \frac{\sigma_{11} - \sigma_{22}}{2} \sin 2\psi \quad (6)$$

for any point along a radial trace. Next, n equally spaced inspection points are selected on the coating along one radial trace. About these inspection points, a plane element $dr, rd\theta$ is designated. In the limit, this element approaches dx, dy (Fig. 1). By arbitrarily choosing $\psi = 1$

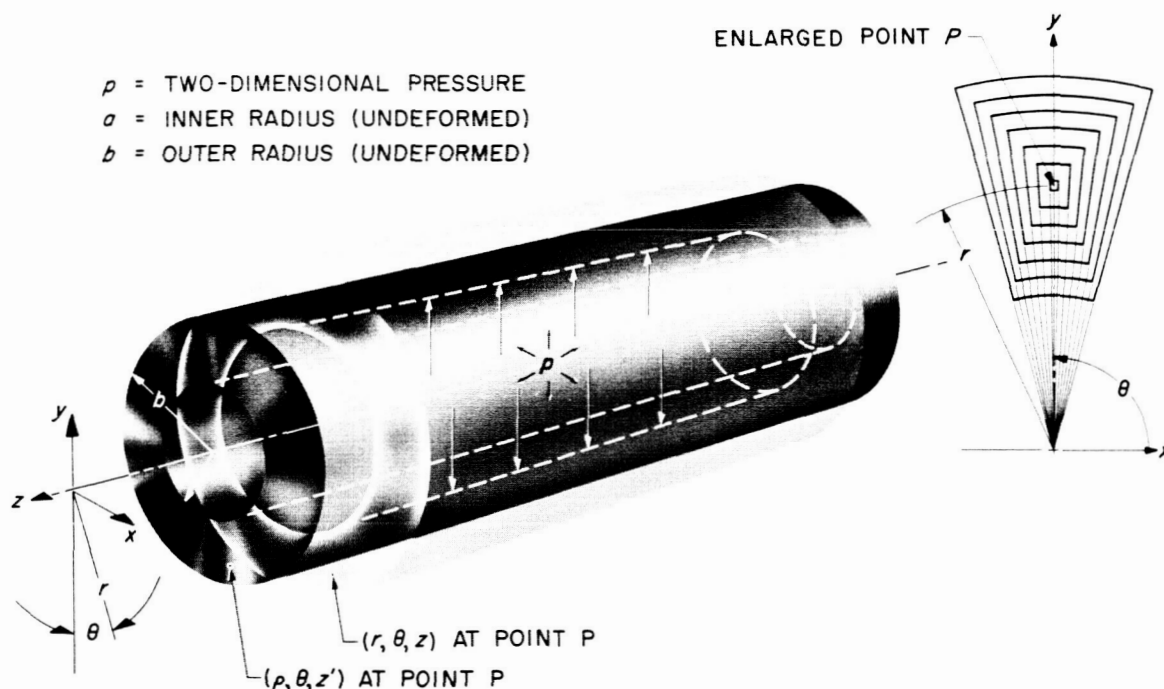


Fig. 1. The deformation of an unrestricted, thick-walled cylinder of solid propellant, by internal pressurization

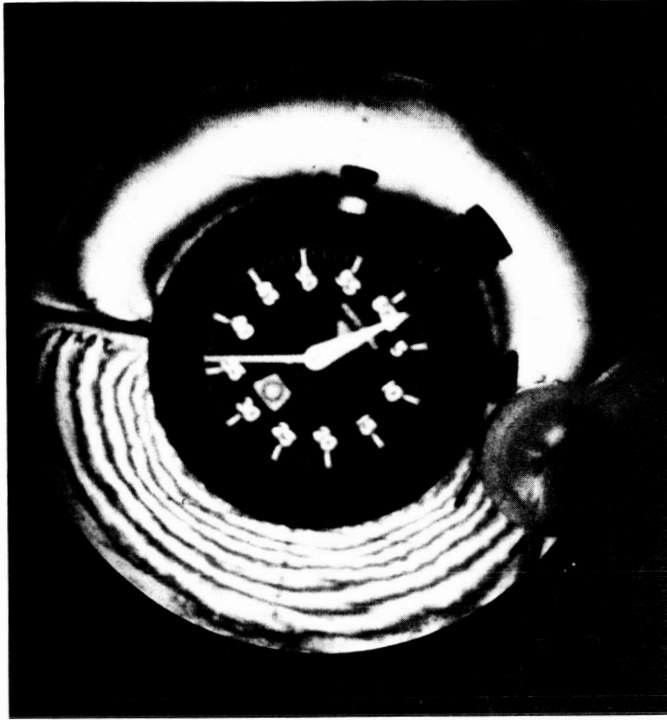


Fig. 2. Two semicoatings of differing sensitivity

deg, Eq. (6) may be applied at the edge of the element (dx, dy) , and thus a shear is obtained parallel to the radial trace $\theta = 90$ deg (Fig. 1). Thus the local shear stress, Eq. (6), with respect to any point i along the radial trace in the Cartesian system, becomes

$$\sigma_{xy}^i = 0.01745 (\sigma_{11} - \sigma_{22})_i \quad (7)$$

The magnitude of $(\sigma_{11} - \sigma_{22})_i$ is obtained directly from the observed color (fringe value) at the point i . This color is converted to stress by means of a calibration curve of color vs. stress, Eq. (1), experimentally established for each photoelastic coating.

It is desirable to reference the shear σ_{xy}^i with respect to the axis of the cylinder. In this manner the fringe value of the isochromatic trace (in psi) can be directly assigned to Eq. (7) since the trace is originally measured with reference to the symmetrical cylinder axes. In Cartesian coordinates, the distance x from a point i on the reference radius ($\theta = 90$ deg) to the parallel shear stress σ_{xy} may be expressed as

$$x_i = 0.01746 [y_n + \delta(n - i)] \quad (8)$$

In the close proximity of the point under investigation (noting that $\sigma_{xy}^i \approx 0$ at $x_i = 0$) the shear σ_{xy}^i with respect to x_i may be approximated in incremental form

$$\frac{\Delta \sigma_{xy}^i}{\Delta x_i} \approx \frac{d\sigma_{xy}^i}{dx_i} \quad (9)$$

From Eq. (5) one notes that

$$\frac{\partial \sigma_{yy}^i}{\partial y_i} = - \frac{\partial \sigma_{xy}^i}{\partial x_i} \quad (10)$$

so that the desired quantities $\partial \sigma_{yy}^i / \partial y_i$ are obtained.

The relationship between σ_{yy}^i and y_i can be obtained on a computer by using Simpson's rule and assuming the boundary conditions $\sigma_{yy}^i = 0$ at y_1 . Separation of the principal stresses from isochromatic data is thus achieved by knowing the calibrated stress-strain relationship of the linear coating.

The principal strains in the coating are then computed from

$$\epsilon_{11}^i = \left(\frac{\sigma_{11}}{E} - \frac{\mu}{E} \sigma_{22} \right)_i \quad (11)$$

$$\epsilon_{22}^i = \left(\frac{\sigma_{22}}{E} - \frac{\mu}{E} \sigma_{11} \right)_i$$

These measurements can be made at different time intervals to measure the creep phenomenon of the material under study.

B. A Method Peculiar to Incompressible Coatings

A second and perhaps less tedious method for reducing the principal strains is predicated upon the fact that a polyurethane resin is essentially incompressible. This experimental observation introduces another equation, thus enabling the computation of the five unknowns, σ_{11} , σ_{22} , ϵ_{11} , ϵ_{22} , and ϵ_{33} . The following five equations are

sufficient to determine the stress-strain-optic state of the coating:

1. The stress-optic law for a urethane resin is

$$\begin{aligned} n_{11} - n_{22} &= 2tC(\sigma_{11} - \sigma_{22}) \\ &= 2t_0 C(1 + e_{33})(\sigma_{11} - \sigma_{22}) \end{aligned} \quad (12)$$

2. Since the coating is incompressible, the strains are related by

$$(1 + \epsilon_{11})(1 + \epsilon_{22})(1 + e_{33}) = 1 \quad (13)$$

3. The classical constitutive equations for plane stress are

$$\begin{aligned} \epsilon_{11} &= \frac{1}{E}(\sigma_{11} - \mu\sigma_{22}) \\ \epsilon_{22} &= \frac{1}{E}(\sigma_{22} - \mu\sigma_{11}) \\ e_{33} &= -\frac{\mu}{E}(\sigma_{11} + \sigma_{22}) \end{aligned} \quad (14)$$

These equations reduce to a nonlinear set that may be solved by the Newton-Raphson method, which can be programmed on a computer. This alternate method for

separating the principal strains ϵ_{11} and ϵ_{22} allows point strain computations without the need for assuming structural boundary conditions. On the other hand, no information regarding principal directions may be had using this approach.

C. Comparison of the Methods

The two methods discussed above for reducing the biaxial principal strains in the coating are expedient for engineering analysis. Viscoelastic strain data can quickly become voluminous, and a decision between the time available to reduce data and the desired accuracy must be made to suit the individual investigation. An estimate of the strain measurement discrepancies among the two proposed methods and a theoretical approximation may be derived from Table 1.

The data used to compute the strains in Table 1 were obtained from an "incompressible" elastic thick-walled cylinder (unfilled pure rubber) whose modulus was of the same order of magnitude as that of solid propellant. The elastic and optic constants of the coatings used were the same for both the shear-difference and incompressibility methods. A perturbation of these experimentally determined constants does not significantly change the values of the strains shown in Table 1.

A comparison between the shear-difference and incompressibility methods indicates a possible discrepancy

Table 1. Biaxial strains obtained by three methods

Computer solution methods				Theoretical approximation in./in.	
Shear-difference method, in./in.		Incompressibility assumption method, in./in.			
ϵ_1	ϵ_2	ϵ_1	ϵ_2	ϵ_1	ϵ_2
0.0009	-0.0010	0.0010	-0.0010	0	0
0.0047	-0.0038	0.0043	-0.0043	0.0079	-0.0056
0.0091	-0.0075	0.0084	-0.0081	0.0138	-0.0097
0.0118	-0.0101	0.0108	-0.0110	0.0190	-0.0134
0.0177	-0.0142	0.0162	-0.0154	0.0241	-0.0170
0.0312	-0.0259	0.0276	-0.0254	0.0311	-0.0219
0.0447	-0.0359	0.0389	-0.0360	0.0396	-0.0279
0.0548	-0.0414	0.0464	-0.0430	0.0454	-0.0320
0.0618	-0.0471	0.0527	-0.0482	0.0524	-0.0369

of 0.01 in./in. for ϵ_1 , whereas a possible discrepancy of 0.002 in./in. is found for ϵ_2 .

The theoretical computation assumes that the strains are being computed at the longitudinal center of an infinitely long cylinder, not at the end of a finite cylinder. Hence a discrepancy should be expected between the theoretical approach and either the shear-difference or the incompressibility approach. The discrepancy between the shear-difference and theoretical approaches is observed to be as high as 0.01 in./in. for ϵ_1 and 0.01

in./in. for ϵ_2 . Similarly, the discrepancy between the incompressibility and theoretical approaches is observed to be as high as 0.008 in./in. for ϵ_1 and 0.01 in./in. for ϵ_2 .

These "discrepancies" actually are masked by scatter in the data and, for present purposes, are not considered serious because the interest here lies in the creep curve fitted through the scatter of the strain readings. On the other hand, the accuracy of the strain reduction can be readily improved if a refinement of the methods suggested above is undertaken.

III. DESCRIPTION OF THE APPARATUS

Figure 3 shows an exploded view of the polariscope. It consists of a 35-mm pulse camera (observer), a circular xenon flashtube (Fig. 4), and crossed Polaroid sheets with auxiliary filters. A schematic diagram of the optical

phenomenon of the reflective polariscope described below is shown in Fig. 5. Eight of these crossed sheets (unit polariscopes) are mounted relative to the flashlamp-specimen plane at different angles on an indexing disk, as shown in Fig. 6. Associated instrumentation consists

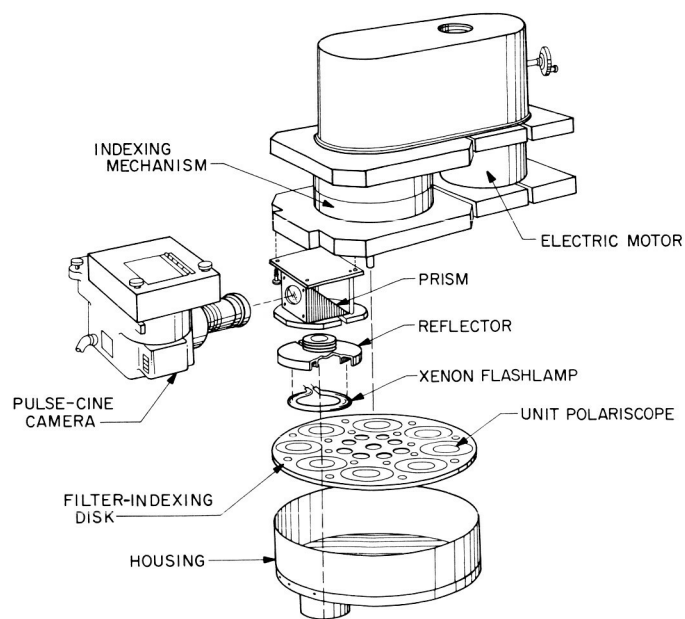


Fig. 3. Exploded view of polariscope

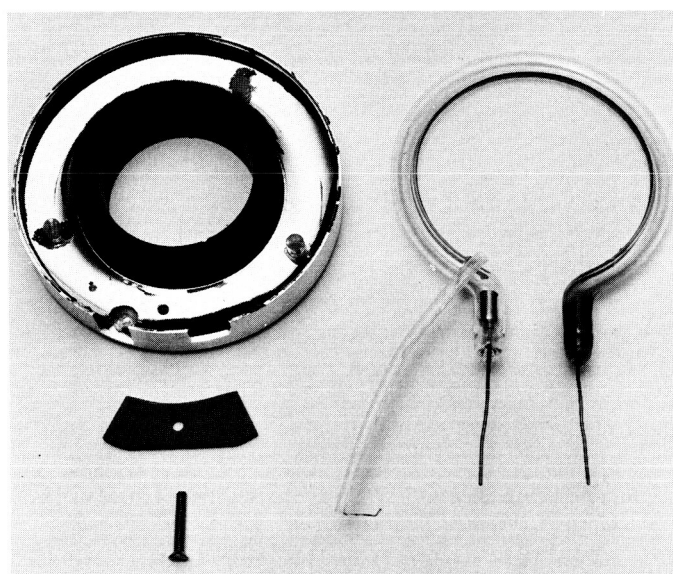


Fig. 4. Torus xenon flashtube and reflector

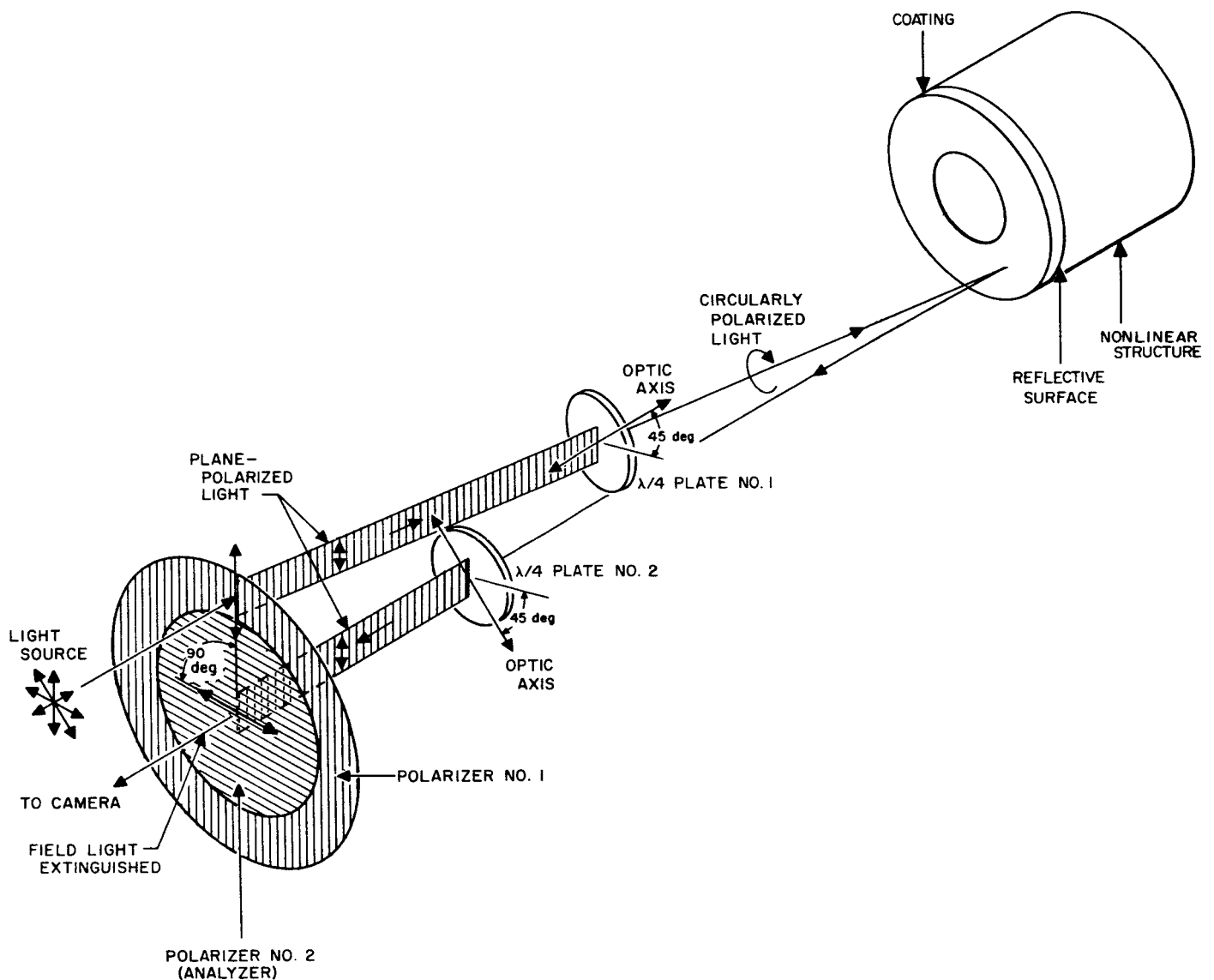


Fig. 5. Reflective polariscope arrangement

of a servo pressurization system and programmable timers to control the propellant grain pressurization as well as the operation of the indexing system (Fig. 7).

A polariscope similar in geometry to the unit polariscope described here was developed by Slot (Ref. 16). This unit consisted of two circular green-fluorescent (monochromatic) tubes. Polaroid filters were attached in such a manner as to allow manual rotation of the system. Hoek (Ref. 17) presented a modified version of Slot's polariscope by using four circular neon (polychromatic) tubes. This apparatus is also designed to be manually rotated. The polariscope unit suggested in this Report (a prototype of which was first considered in Ref. 18) is

much smaller than the polariscopes mentioned above, because of the use of a single xenon-lamp light source.

A. Xenon Flashtube Light Source

Polychromatic light was initially chosen over monochromatic light to study a class of problems, because the strain data reduction was somewhat simplified. A clear distinction between isochromatics and isoclinics was a necessary condition to be satisfied. Monochromatic light can be employed, however, when a particular investigation requires its usage. The choice between these two light sources is also dependent on the low-modulus birefringent resin to be used; i.e., white light for resins of

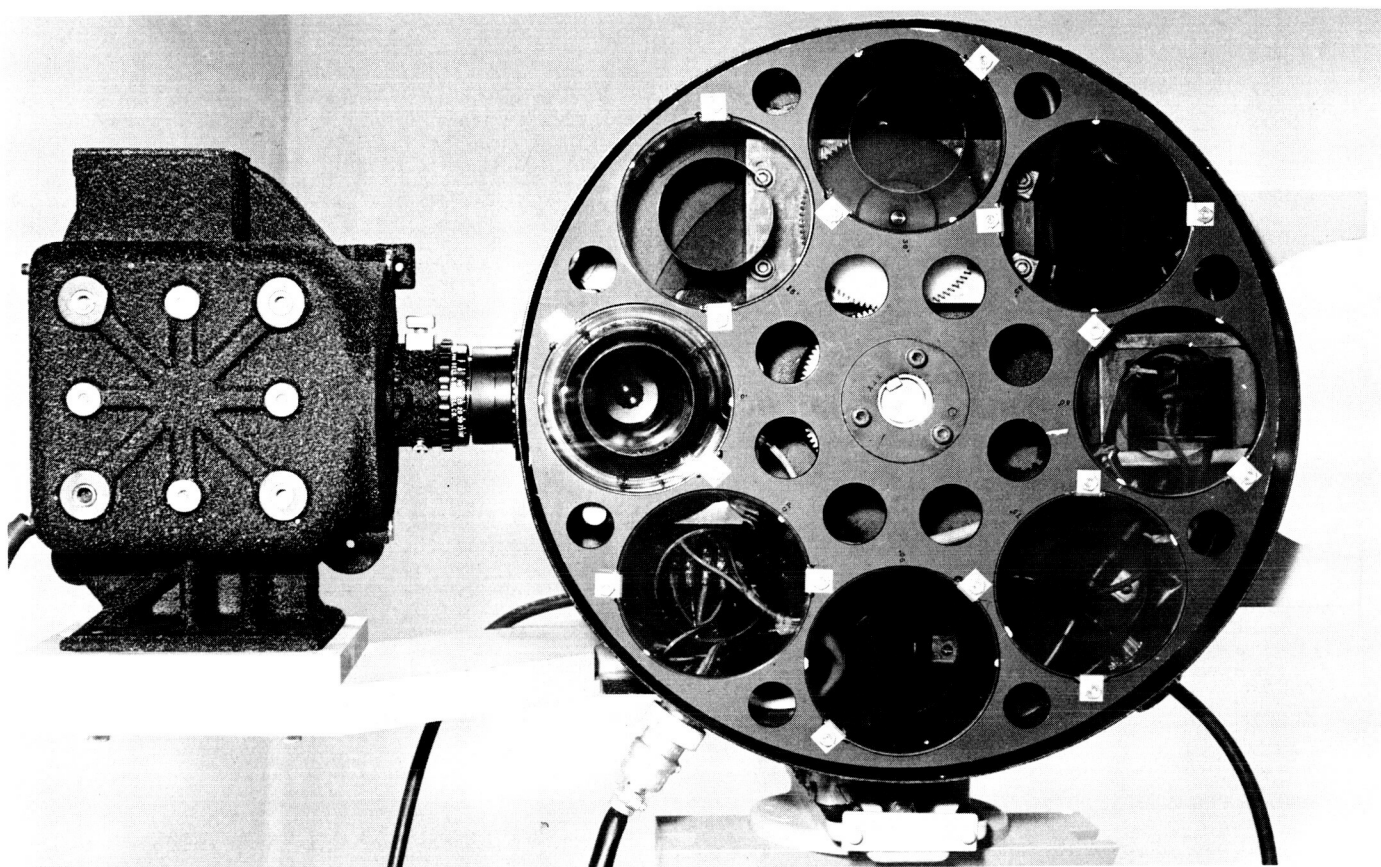


Fig. 6. Various oriented Polaroid filters mounted on an indexing disk

low sensitivity, and monochromatic light for resins of high sensitivity. Monochromatic light may be approximated from white light by the use of appropriate filters.

Commercial light sources with a torus geometry are readily available as flash units. Construction of such lamps can also be ordered at a nominal cost. A xenon lamp with an annular diameter of 3 in. and a tube diameter of $\frac{1}{4}$ in. was fitted to a reflector (Fig. 4). A modified Chadwick-Helmuth Strobex Model 121 provided a high-voltage power supply. This supply provides to the lamp a maximum power of 12 w-sec at 5 flashes per second. The power supply is triggered directly from the midshutter contactor of the pulse camera (Fig. 8). In this manner, synchronization between light flash and camera is obtained. The effective flash duration of the xenon lamp is approximately 300 μ sec. The xenon light spectrum is shown in Fig. 9. An interesting comparison between white light (daylight) and xenon-emitted light is shown in Fig. 10. It is noted from this Figure that xenon approximates white light rather well, an important factor in converting observed fringe color to retardation

(Ref. 19). Figure 11 shows the operational design limitations with respect to flash duration time and light energy output for various voltage-capacitance power supplies.

B. Filter-Indexing Mechanism

The basic requirement of an indexing mechanism was to position at rest, in the field of view of a camera, variously oriented Polaroid filters. Eight separate crossed-Polaroid systems (Fig. 5) were deemed sufficient to obtain an isoclinic plot, at a given strain level and reference time ($t = t_i$), within a short period of time (Δt). Each Polaroid system consists of a disk-shaped analyzer mounted within a ring-shaped polarizer. The two filters may be cut from a large Polaroid sheet by means of a steel rule die. They can then be cemented together in a single sheet, noting that their optical axes should be either parallel or crossed. These Polaroid systems are oriented with respect to each other by mounting the systems in a master disk (Fig. 6). This disk is mounted to an indexing mechanism (Fig. 3). A single photograph

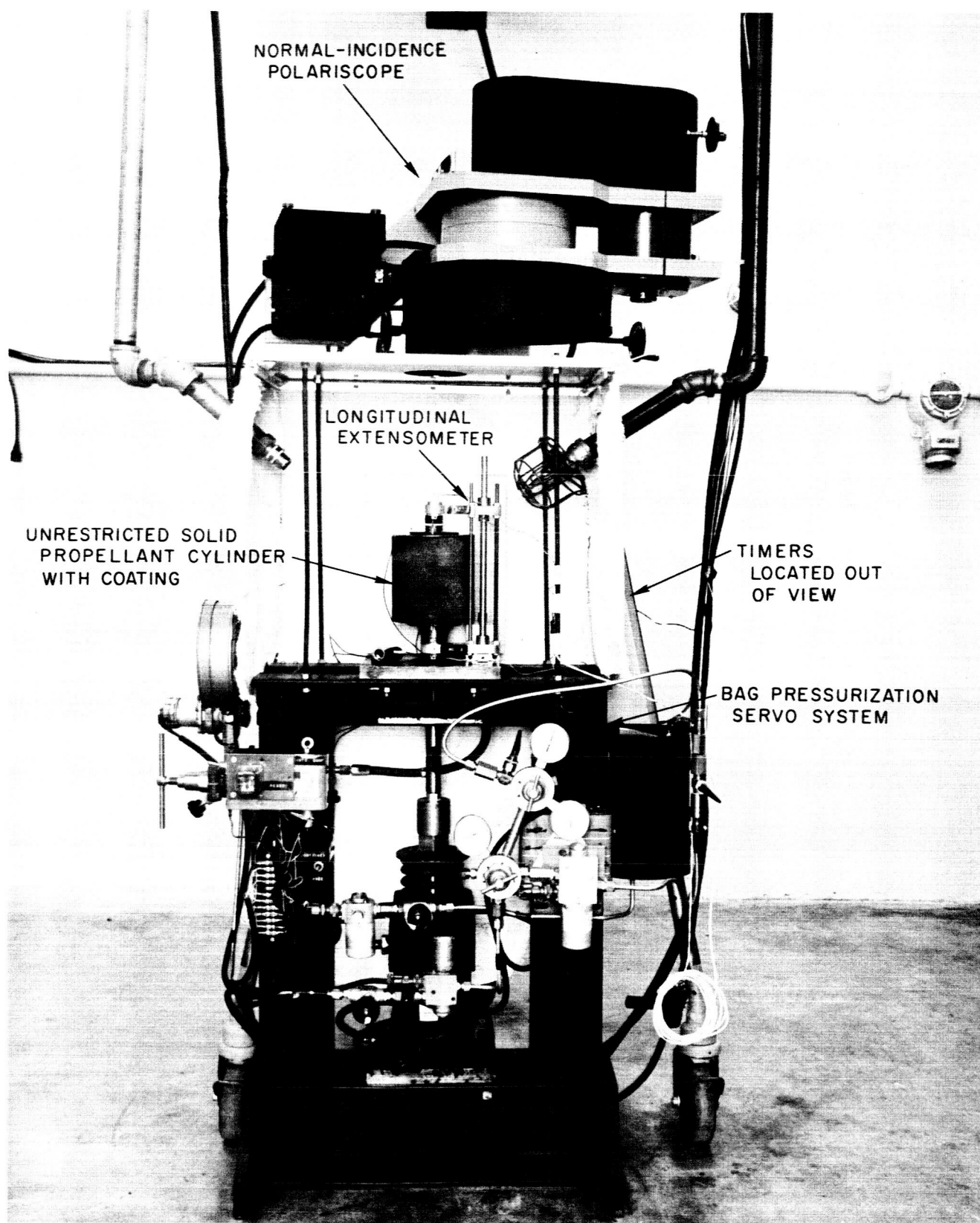


Fig. 7. Polariscope with associated instrumentation

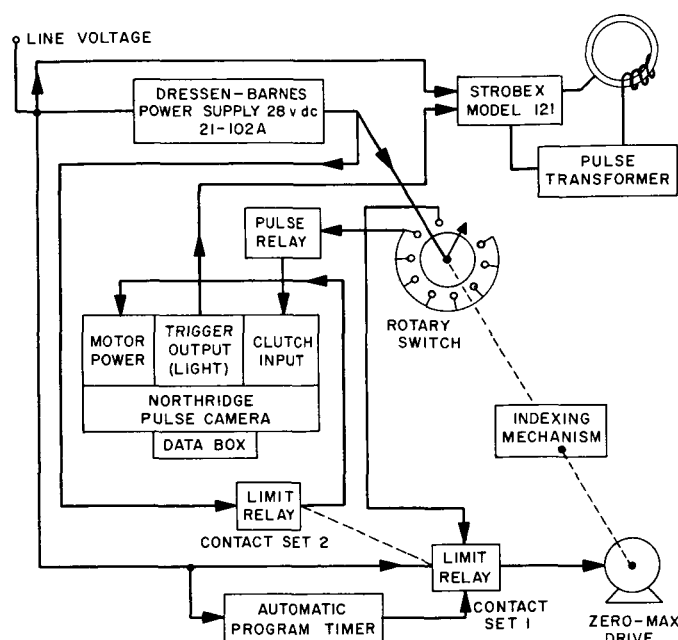


Fig. 8. Electrical schematic of polariscope

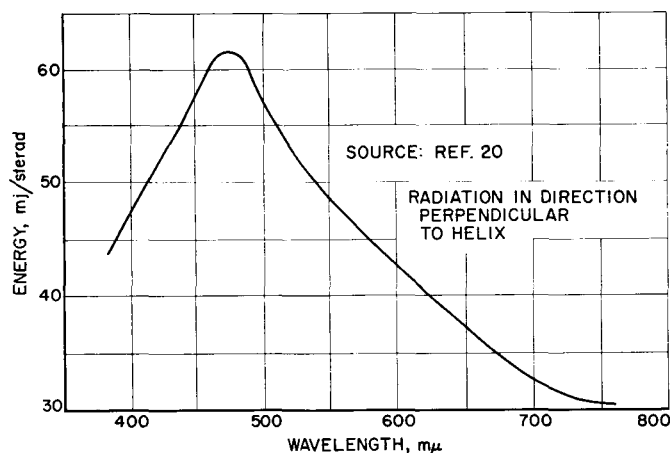


Fig. 9. Spectral energy distribution curve of a typical xenon-filled flashtube

may thus be exposed for each of the various orientations of the Polaroid filters.

An indexing mechanism of the sealed-Tangen-drive type was chosen because of its smooth action and positive indexing. This unit provides 90 deg of rotation for indexing and 270 deg of dwell per 360 deg of input rotation. A 2:1 gear ratio produces eight indexes (each of 45 deg) per full revolution of the input drive: seven filter stops, each oriented 15 deg with respect to one another, and one filter stop using quarter-wave plates mounted

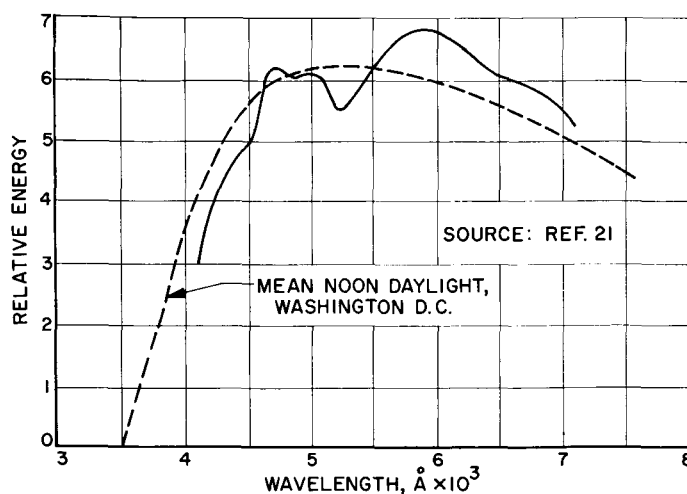
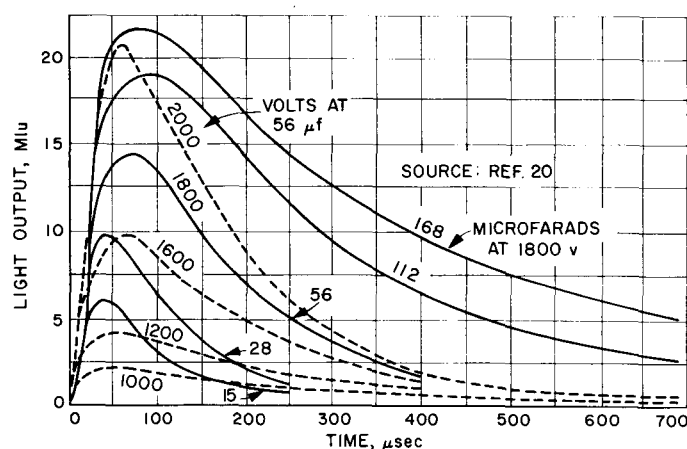


Fig. 10. Spectral energy distribution of xenon-filled tubes under normal loading



indexed position, only one photograph was taken. In addition, the camera had to provide a mid-shutter triggering pulse to the Strobex power supply for light synchronization. The camera was also provided with a data box attachment that recorded film sequence number and running time. These data are recorded in the sprocket area of the film.

D. Program Timing

Three timing ranges were considered sufficient to study a large class of viscoelasticity problems. The first timing range may be varied from 0 to 15-hr duration; within this duration, equal increment periods from 15 sec to 15 min can be chosen to initiate the polariscope operation. The second timing range may be varied from 0 to 60-hr duration; within this duration, equal increment periods from 2 min to 2 hr can similarly be chosen to initiate the polariscope operation. Automatic flip-flop circuitry provides sampling between the first and second

ranges. A third range may be varied from 0 to 60 hr. This control turns off the polariscope at any prescribed time.

E. Apparatus Summary

A basic design philosophy underlying the polariscope (Fig. 3, 7) was to insure positiveness of position. Since it was decided that a minimum of eight photographs was desirable to define the surface strains at any time t , each photograph was mechanically linked through the entire system. Under these circumstances, any photograph may be easily identified with respect to loading conditions and time.

Summarizing the operation, eight Polaroid filters in all are used to map the isoclinics for a given value of the isochromatic. The operation is then repeated at various times to obtain biaxial strains as a function of time.

IV. AN ILLUSTRATIVE EXAMPLE AND DISCUSSION

Multiaxial creep data in a point region located at the radial center of the bonded coating (Fig. 1) were obtained from an unrestricted, pressurized, thick-walled cylinder of polyurethane solid propellant and are shown in Fig. 12a, b, and c. The biaxial coating data are shown in Fig. 12a and b. The longitudinal strain data were obtained by monitoring the contraction of the unrestricted cylinder with a simple resistance extensometer and are shown in Fig. 12c. The curves have the well-known characteristics associated with creep data. The question as to accuracy has been experimentally resolved elsewhere (Ref. 6, 15) for this test and is in the same realm as that discussed in Ref. 16 and 17. As in most experiments, the accuracy may be readily improved, subject to the law of diminishing returns. The strain discrepancy for the strains presented here can conservatively be taken as less than 10%, i.e., $\epsilon_{11} = 0.09 \pm 0.009$.

A note regarding the separation of the biaxial principal strains is in order. It should be recognized that Eq. (1) through (11) assume that the classical photoelasticity

phenomenon exists. This requires a known relationship among the stresses, strains, and retardation. If a material does not exhibit classical photoelasticity, then the polariscope described in this Report is applicable for recording isoclinics and isochromatics as a function of time. For this general situation, new constitutive stress-strain-optic equations must be hypothesized (Ref. 13, 14).

The applicability of Eq. (12), (13), and (14) is even more restrictive, since they require the photoelastic coating to be incompressible. No information is given with regard to the direction of the principal strains or stresses. Another serious disadvantage is that this set of nonlinear equations does not have a unique solution. Hence, if these simpler equations are used, the direction of principal stresses or strains, as well as a reasonable approximation of their magnitude, must be known *a priori*. These latter conditions were satisfied in this study by using a symmetrical test specimen. The stresses in the coating were initially approximated by the classical cylinder equations.

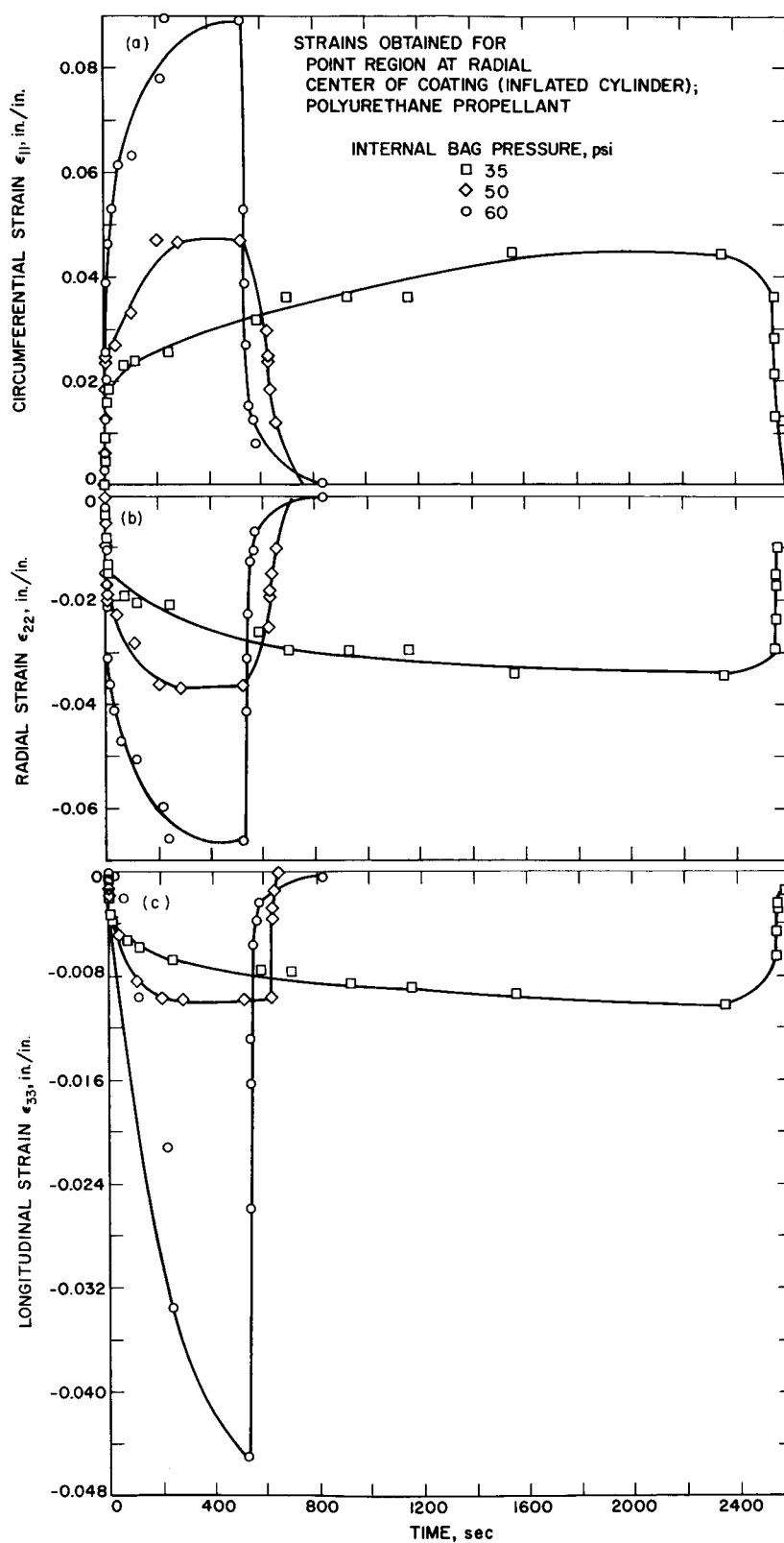


Fig. 12. Circumferential, radial, and longitudinal strains vs. time

V. CONCLUSION

A normal-incidence reflective polariscope to measure viscoelastic strains has been described. Two restrictive methods to reduce the principal strains in a birefringent

coating were also presented. Creep data obtained for polyurethane propellant illustrate the potential of such an instrument in the field of mechanical properties study.

ACKNOWLEDGMENT

The authors wish to acknowledge the advice and technical support of V. H. Culler and J. I. Watstein.

NOMENCLATURE

C	stress-optic constant, psi^{-1}	x, y, z	Cartesian coordinate system (z thickness of coating)
E	Young's modulus, psi	δ	equal increment on the radial trace $= (y_1 - y_n)/(n - 1)$
K	strain-optic constant	ϵ_{11}	principal strain in the 11 privileged direction
e_{33}	thickness strain of the coating	ϵ_{22}	principal strain in the 22 privileged direction
m_{ijkl}	36 possible elastic constants, psi	ϵ_{33}	longitudinal strain of the thick-walled cylinder
n	number of points being investigated	ϵ_{kl}	strain tensor
n_{11}	refractive index in the 11 privileged direction	θ	reference angle, deg
n_{22}	refractive index in the 22 privileged direction	μ	Poisson's ratio
t	coating thickness at any state of strain, in.	σ_{11}	principal stress in the 11 privileged direction
t_0	original coating thickness, in.	σ_{22}	principal stress in the 22 privileged direction
x_i	distance from a point i on the reference radial trace to the shear plane Ψ , in.	σ_{ij}	stress tensor
y_n	distance from symmetrical center of cylinder to point under investigation, in.	σ_Ψ	shear stress, psi
		Ψ	angle at which shear acts, deg

REFERENCES

1. Ferry, J. D., *Viscoelastic Properties of Polymers*, John Wiley and Sons, New York, 1961.
2. Eringen, A. C., *Nonlinear Theory of Continuous Media*, McGraw-Hill, Inc., New York, 1962, Chapter 10.
3. *Viscoelasticity*, ed. by J. T. Bergen, Academic Press, New York, 1960.
4. Bland, D. R., *The Theory of Linear Viscoelasticity*, Pergamon Press, New York, 1960.
5. San Miguel, A., "Propellant Strain Analysis by the Photoelastic Coating Technique," *Bulletin of the Twentieth Meeting, JANAF Solid Propellant Information Agency*, The Johns Hopkins University, Silver Spring, Maryland, November 1961.
6. San Miguel, A., *An Experimental Method to Measure the Strain Energy Function W*, Technical Report No. 32-365, Jet Propulsion Laboratory, Pasadena, California, December 20, 1962.
7. Zandman, F., Redner, S. S., and Post, D., "Photoelastic Analysis in Thermal Fields," *Experimental Mechanics*, Vol. 3, No. 9, 1963.
8. San Miguel, A., and Duran, E. N., "Some Low-Modulus Birefringent Resins," *Experimental Mechanics*, Vol. 4, No. 3, 1964.
9. Zandman, F., Redner, S. S., and Riegner, E. I., "Reinforcing Effect of Birefringent Coatings," *Experimental Mechanics*, Vol. 2, No. 2, 1962.
10. Lee, T. C., Mylonas, C., and Duffy, J., "Thickness Effects in Birefringent Coatings with Radial Symmetry," *Experimental Mechanics*, Vol. 1, No. 10, 1961.
11. Duffy, J., "Effects of the Thickness of Birefringent Coatings," *Experimental Mechanics*, Vol. 1, No. 3, 1961.
12. Post, D., and Zandman, F., "Accuracy of Birefringent-Coating Method for Coatings of Arbitrary Thickness," *Experimental Mechanics*, Vol. 1, No. 1, 1961.
13. Dill, E. H., *On the Theory of Photoviscoelasticity*, Report 63-1, College of Engineering, University of Washington, January, 1963.
14. Gerard, G., "Progress in Photothermoelasticity," *Photoelasticity*, ed. by M. M. Frocht, Pergamon Press, New York, 1963.
15. San Miguel, A., "Continued Studies with the Inflated Cylinder Test via Continuous Media Theory," *Bulletin of the Second Meeting of ICRPG Working Group on Mechanical Behavior*, November 15, 1963, SPIA, The Johns Hopkins University, Applied Physics Laboratory, Silver Spring, Maryland. CONFIDENTIAL
16. Slot, T., "Reflection Polariscope for Photography of Photoelastic Coatings," *Experimental Mechanics*, Vol. 2, No. 2, February 1962 (Presented October 19-21, 1960).
17. Hoek, E., and Bieniawski, X. T., "A Large Field Reflective Polariscope," *The South African Mechanical Engineer*, Vol. 12, No. 8, December 1962.
18. San Miguel, A., "Viscoelastic Strain Analysis by the Photoelastic Coating Technique," *Quarterly Summary Report No. 38-3*, Jet Propulsion Laboratory, Pasadena, California, January 1, 1961. CONFIDENTIAL

REFERENCES (Cont'd)

19. Bloss, R. D., *An Introduction to the Methods of Optical Crystallography*, Holt, Reinhart, and Winston, Inc., New York, 1961.
20. Aspden, R. L., *Electronic Flash Photography*, Temple Press Limited, London, 1959, pp. 46, 47.
21. Illuminating Engineering Society, *IES Lighting Handbook*, New York, 1959, pp. 8-42.